Acta Crystallographica Section F
Structural Biology and Crystallization Communications
ISSN 1744-3091

Structure of 1-deoxy-D-xylulose 5-phosphate reductoisomerase in a quaternary complex with a magnesium ion, NADPH and the antimalarial drug fosmidomycin

Shunsuke Yajima,[a]* Kodai Hara,[a]‡ Daisuke Iino,[a] Yasuyuki Sasaki,[a] Tomohisa Kuzuyama,[b] Kanju Ohsawa[a] and Haruo Seto[c]

[a]Department of Bioscience, Tokyo University of Agriculture, Setagaya-ku, Tokyo 156-8502, Japan, [b]Biotechnology Research Center, University of Tokyo, Bunkyo-ku, Tokyo 113-8657, Japan, and [c]Department of Applied Biology and Chemistry, Tokyo University of Agriculture, Setagaya-ku, Tokyo 156-8502, Japan

‡ Current address: Field of Supramolecular Biology, International Graduate School of Arts and Sciences, Yokohama City University, Tsurumi-ku, Yokohama 230-0045, Japan.

Correspondence e-mail: yshun@nodai.ac.jp

Received 1 March 2007
Accepted 18 May 2007

PDB Reference: 1-deoxy-D-xylulose 5-phosphate reductoisomerase complex, 2egh, r2eghsf.

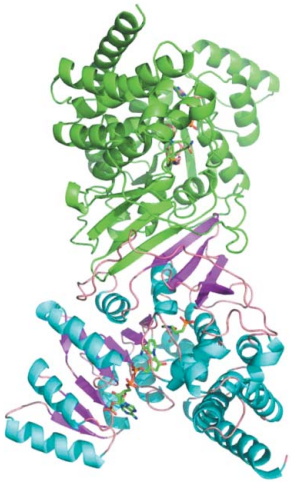

The crystal structure of 1-deoxy-D-xylulose 5-phosphate reductoisomerase (DXR) from *Escherichia coli* complexed with Mg^{2+}, NADPH and fosmidomycin was solved at 2.2 Å resolution. DXR is the key enzyme in the 2-*C*-methyl-D-erythritol 4-phosphate pathway and is an effective target of antimalarial drugs such as fosmidomycin. In the crystal structure, electron density for the flexible loop covering the active site was clearly observed, indicating the well ordered conformation of DXR upon substrate binding. On the other hand, no electron density was observed for the nicotinamide-ribose portion of NADPH and the position of Asp149 anchoring Mg^{2+} was shifted by NADPH in the active site.

1. Introduction

Isopentenyl diphosphate (IPP), which is a fundamental unit for the synthesis of terpenoids such as steroid hormones, carotenoids, ubiquinone and menaquinone, is a key compound in all living organisms (Sacchettini & Poulter, 1997). In mammals, IPP is synthesized by the mevalonate pathway starting from acetyl-CoA, whereas in eubacteria, plastids of higher plants and malaria parasites this compound is formed through the 2-*C*-methyl-D-erythritol 4-phosphate (MEP) pathway (Rohmer, 1999; Kuzuyama & Seto, 2003), which starts with the condensation of pyruvate and glyceraldehyde-3-phosphate to produce 1-deoxy-D-xylulose 5-phosphate (DXP) by DXP synthase.

In the second step of the MEP pathway, 1-deoxy-D-xylulose 5-phosphate reductoisomerase (DXR; EC 1.1.1.267) converts DXP to MEP by intramolecular rearrangement and reduction using a divalent cation, namely Mg^{2+}, Mn^{2+} or Co^{2+}, and the cofactor NADPH (K_m = 18 μ*M* with Mg^{2+}, 7.4 μ*M* with Mn^{2+} or 8.8 μ*M* with Co^{2+}; Kuzuyama, Shimizu *et al.*, 1998; Takahashi *et al.*, 1998). Furthermore, five other enzymes are necessary to produce the final products IPP and dimethylallyl diphosphate (DMAPP), which are interconverted by IPP isomerase.

As this pathway does not exist in mammals, it has been thought to be an effective drug target. In fact, it has been shown that fosmidomycin effectively inhibits the enzymatic activity of DXR from *Escherichia coli* (K_i = 38 n*M* in a mixed inhibition pattern; Kuzuyama, Takahashi *et al.*, 1998); furthermore, this drug has been demonstrated to cure rodent malaria caused by *Plasmodium vinckei* (Jomaa *et al.*, 1999) and has been used to cure uncomplicated *P. falciparum* malaria in humans (Wiesner *et al.*, 2003; Lell *et al.*, 2003). In order to obtain clues to the design of new drugs and to understand the catalytic mechanism, several crystal structures of DXR with or without cofactors and/or substrates/inhibitors have been reported. These structures include the apo form of DXR from *E. coli* (Reuter *et al.*, 2002), DXR complexed with a sulfate ion and NADPH (Yajima *et al.*, 2002), DXR complexed with a bisphosphonate ion and a sulfate ion (Yajima *et al.*, 2004), DXR complexed with Mn^{2+} and fosmidomycin (Steinbacher *et al.*, 2003), DXR complexed with NADPH and DXP, and DXR complexed with NADPH and fosmidomycin (Mac Sweeney *et al.*, 2005). The structures of DXR from *Zymomonas mobilis* complexed with NADPH (Ricagno *et al.*, 2004) and from *Mycobacterium tuberculosis*

complexed with a sulfate ion (Henriksson *et al.*, 2006) have also been reported. However, the complete structure of DXR complexed with NADPH, a divalent cation and a substrate/inhibitor has not yet been reported. Here, we report for the first time the structure of DXR from *E. coli* in a quaternary complex with Mg^{2+}, NADPH and fosmidomycin. This crystal structure provides information on the active site of DXR.

2. Materials and methods

2.1. Purification and crystallization

The *E. coli* DXR protein was overexpressed in *E. coli* and purified as reported previously (Yajima *et al.*, 2002). DXR has a six-histidine tag at the N-terminus in the pQE30 vector (Qiagen) and was purified using a Ni-chelate column (GE Healthcare) followed by purification on a DEAE Toyopearl column (Tosoh Co.). The purified protein was concentrated to approximately 80 mg ml^{-1} in a buffer containing 20 m*M* Tris–HCl pH 8.5, 100 m*M* KCl and 10% glycerol. The purified protein was mixed in a 1:1 ratio with crystallization buffer [0.1 *M* sodium citrate pH 5.6, 1 *M* $(NH_4)_2SO_4$, 0.01 *M* sodium potassium tartrate, 4.17 m*M* dithiothreitol, 1 m*M* $MgCl_2$ and 6.25 m*M* NADPH] and subjected to the hanging-drop vapour-diffusion method at 277 K. This crystallization condition was obtained by a minor modification of one determined previously (Yajima *et al.*, 2004). Crystals appeared within a few days and continued to grow for approximately one week.

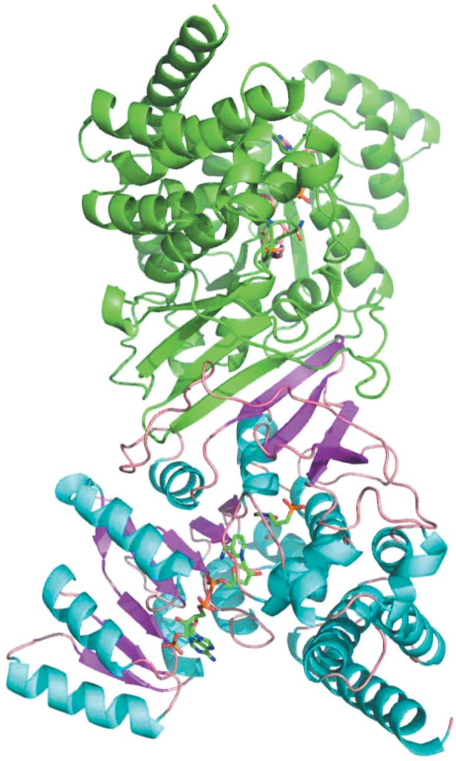

Figure 1
Overall structure of DXR. The homodimeric structure of DXR is shown: one subunit (top) is coloured green, while the other subunit (bottom) is coloured turquoise and purple according to its secondary structure. NADPH and fosmidomycin atoms are shown as sticks. All colour figures in this paper were prepared using *PyMol* (DeLano, 2002).

Table 1
Data-collection and refinement statistics.

Values in parentheses are for the highest resolution shell.

Data collection	
Unit-cell parameters (Å)	a = 180.5, b = 59.1, c = 87.1
Space group	$P2_12_12$
Resolution (Å)	50–2.2 (2.28–2.20)
Unique observed reflections	90406 (10158)
Redundancy	4.9 (4.6)
Completeness (%)	98.3 (98.0)
R_{merge}	0.104 (0.682)
$I/\sigma(I)$	9.8 (2.6)
Refinement	
Resolution (Å)	47.2–2.2 (2.34–2.20)
No. of reflections	88258 (14874)
R_{work}/R_{free}	0.218/0.225 (0.287/0.290)
R.m.s.d. from ideal geometry	
Bonds (Å)	0.010
Angles (°)	1.9
Dihedrals (°)	21.2
Impropers (°)	1.19
No. of atoms/average B factor (Å^2)	
Protein atoms	6063/39.5
Water molecules	299/38.1
Fosmidomycin atoms	22/77.4
Mg atoms	2/59.5
NADPH atoms	96/74.8
Ramachandran plot	
Favoured (%)	91.6
Additionally allowed (%)	8.0
Generously allowed (%)	0.4

2.2. Data collection and structure determination

The DXR crystals were soaked in a cryoprotectant buffer for 5 min before flash-cryocooling. This buffer was a solution of 25% glycerol, 50 m*M* NADPH, 0.96 *M* $MgCl_2$ and 1 *M* fosmidomycin in the crystallization buffer.

Data were collected at beamline BL6A, Photon Factory and were processed with *DENZO*/*SCALEPACK* (Otwinowski & Minor,

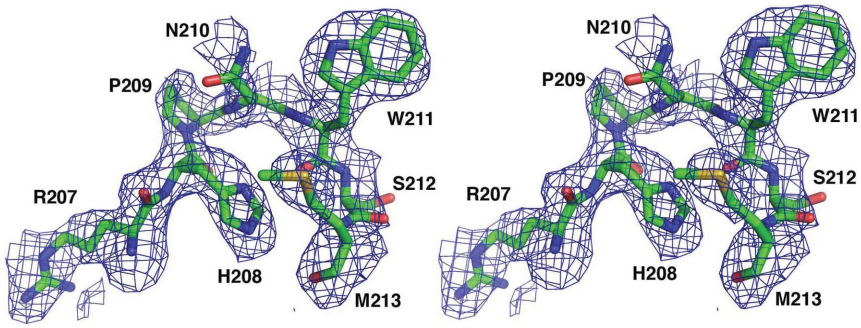

Figure 2
Stereo representation of the flexible loop region. An $F_o - F_c$ OMIT map of the flexible loop region spanning Arg207–Met213 is shown. The contour level is 1.0σ.

1997). The initial electron-density map was calculated using *CNS* (Brünger *et al.*, 1998) using the coordinates of the DXR structure (PDB code 1jvs). Since the electron-density map obtained at this point was very clear, noncrystallographic symmetry restraints were not used throughout the refinement. The model was refined by using the simulated-annealing, conjugate-gradient minimization and individual *B*-factor minimization procedures available in *CNS*. A series of OMIT maps systematically excluding a small part of the model were also used. The model was built and adjusted using the program *QUANTA* (Accelrys, Inc.). R_{free} was calculated with 5% of the reflections that were set aside randomly throughout the refinement.

3. Results and discussion

3.1. Overall structure

To obtain the complex structure, we attempted to soak the crystals in the Mg^{2+}, Mn^{2+} or Co^{2+} solution, since all these ions can serve as a cofactor for the catalytic reaction of DXR. However, both Mn^{2+} and Co^{2+} ions destroyed the crystals upon soaking and only the Mg^{2+} ion was successfully incorporated into the crystals. Since the high *B*-factors of the Mg^{2+} ions (~60 Å^2) indicated low occupancies, we tried to soak the crystals for a longer time, but this resulted in lower resolution data. We also used 1 *M* fosmidomycin because $(NH_4)_2SO_4$ at 1 *M* concentration in the crystallization buffer easily produces the sulfate ion-bound DXR crystal; in this crystal, the sulfate ion occupies the position at which the phosphonate group of fosmidomycin binds at the active site, as observed in the previously reported DXR structure (Yajima *et al.*, 2002). In fact, since a higher concentration of the DXR protein was used in this study, the concentration of $(NH_4)_2SO_4$ was less than that used previously.

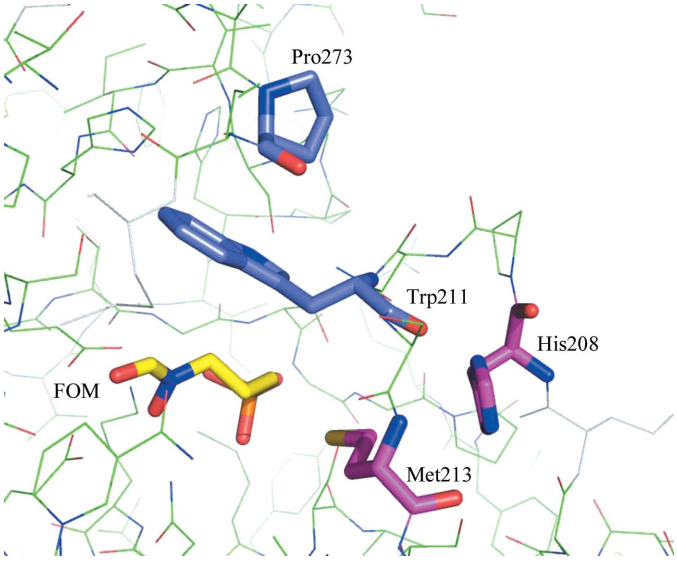

Figure 3
Hydrophobic interactions of fosmidomycin with the residues in DXR. Fosmidomycin is labelled FOM. There are two modes of hydrophobic interaction to achieve the well ordered conformation of the loop region. One is Pro273–Trp211–FOM and the other is His208–Met213–FOM.

The complex structure of *E. coli* DXR with Mg^{2+}, NADPH and fosmidomycin was obtained and refined at 2.2 Å resolution with an R_{work} and R_{free} of 0.218 and 0.225, respectively. The refinement statistics are summarized in Table 1. The DXR structure was composed of a homodimer (716 observed residues) in the asymmetric unit. A Ramachandran analysis using the program *PROCHECK* (Laskowski *et al.*, 1993) showed that 656 residues (91.6%) were in the most favoured regions, 57 (8.0%) were in the additionally allowed region and three (0.4%) were in the generously allowed region. Of the three residues in the additionally allowed region, Asn210 in chain *A* is located in the flexible loop region and Ser257 is located at the end of a β-strand in both chains. Since the complex structure was obtained by the soaking method, the overall structure was the same as that reported previously for DXR, in which the monomer structure comprised three domains: an NADPH-binding domain, a central catalytic domain and a C-terminal α-helical domain. Furthermore, the monomers constitute the homodimer structure by forming a β-sheet with β-strands from each monomer at the dimer interface (Fig. 1).

3.2. The active site and the flexible loop

In the active site, we could observe electron density for Mg^{2+}, fosmidomycin and half of the NADPH molecule. The region spanning His208–Met213 is considered to be the flexible loop that functions to open/close the active site of DXR. In the crystal structure of the apo form of DXR (Reuter *et al.*, 2002) the loop is open, whereas in the crystal structures of DXR bound to a sulfate ion (Yajima *et al.*, 2002) or an inhibitor (Steinbacher *et al.*, 2003) the loop covers the

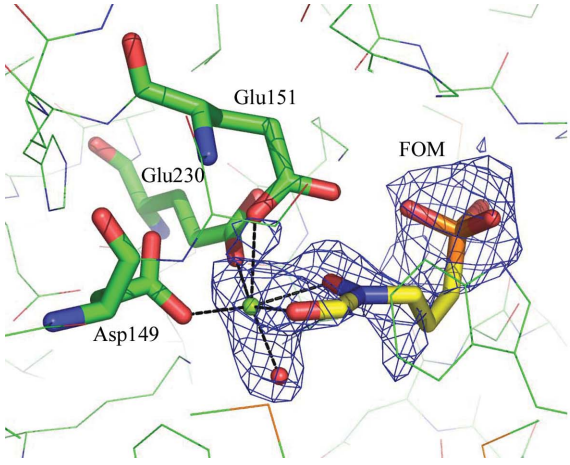

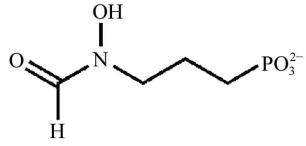

Figure 4
The octahedral coordination of Mg^{2+}. In the active site of DXR, Mg^{2+} (green sphere) is octahedrally coordinated by Asp149, Glu151, Glu230, a water molecule (red sphere) and fosmidomycin. An $F_o - F_c$ OMIT map of fosmidomycin, Mg^{2+} and a water molecule is also shown at a contour level of 1.0σ. The map was calculated by excluding fosmidomycin, Mg^{2+} and the water molecule from the model using *CNS*. The chemical structure of fosmidomycin is shown on the right.

active site as a lid. However, it was reported that electron density for this loop in the abovementioned complex structures could not be observed clearly, except in the ternary complex of *E. coli* DXR with NADPH and fosmidomycin, which formed a tight-binding closed conformation (PDB code 1q0l; space group $P3_121$, unit-cell parameters $a = b = 109.14$, $c = 91.29$ Å; Mac Sweeney *et al.*, 2005). In the quaternary complex structure investigated in this study, the electron density of the loop region was clearly observed (Fig. 2). This was achieved mainly through hydrophobic interactions, in which Trp211 in the loop was sandwiched between Pro273 and the backbone of fosmidomycin and Met213 in the loop interacted with the backbone of fosmidomycin. Met213 also interacted hydrophobically with the imidazole side chain of His208 in the loop (Fig. 3). Thus, fosmidomycin contributed greatly to the formation of the well ordered loop conformation.

When the binding mode of fosmidomycin was examined, it was found that the drug was tightly bound in the active site by several interactions, including the abovementioned hydrophobic contacts. Ser185, Ser221 and Lys227, which are highly conserved residues (Kuzuyama *et al.*, 2000), formed hydrogen bonds to the O atoms of the phosphonate group; Asp149, Glu151 and Glu230, which are also highly conserved residues (Kuzuyama *et al.*, 2000) in the active site, formed hydrogen bonds to the (*N*-formyl-*N*-hydroxy)amino group. Mg^{2+} is liganded by the (*N*-formyl-*N*-hydroxy)amino group and is octahedrally coordinated overall in a shell formed by ligand atoms from Asp149, Glu151, Glu230, a water molecule and fosmidomycin (Fig. 4). This coordination was the same as that observed for Mn^{2+} in the ternary complex of *E. coli* DXR with NADPH (PDB code 1onp; space group $P2_1$, unit-cell parameters $a = 90.8$, $b = 52.3$, $c = 107.6$ Å, $\beta = 92.1^\circ$; Steinbacher *et al.*, 2003). However, the positions of the two metal ions and the water molecules were not identical relative to the (*N*-formyl-*N*-hydroxy)amino group, as explained in the next section.

DXR requires NADPH but not NADH for its activity. In the structure investigated in this study, the pentose phosphate of adenine formed five hydrogen bonds to Thr9, Gly10 and Gly35 and the adenine ring interacted hydrophobically with Ile100 and Ala104. On the other hand, no electron density was observed for nicotinamide-sugar moieties (Fig. 5). This binding mode is different from that observed in the DXR structure with a sulfate ion (PDB code 1jvs), in which the electron density of the entire NADPH molecule was observed. It is reported that electron density for this portion was observed in the ternary complex structure with NADPH and the substrate DXP (PDB code 1q0q) but was not observed in the structure with NADPH and fosmidomycin (PDB code 1q0l). Our result appears to be in agreement with that of 1q0l. However, there is a possibility that the lack of electron density may be caused by the Mg^{2+} binding in the quaternary complex as the distances between the C4/C5 atoms of the nicotinamide ring and the O atom of the *N*-formyl group in fosmidomycin are 3 Å in the ternary structure, which could be close enough to affect the NADPH binding. If this is the case, in the quaternary structure, in which the corresponding distances are 4.5 and 4.2 Å, the Mg^{2+} binding could induce flexibility of the nicotinamide-sugar moieties.

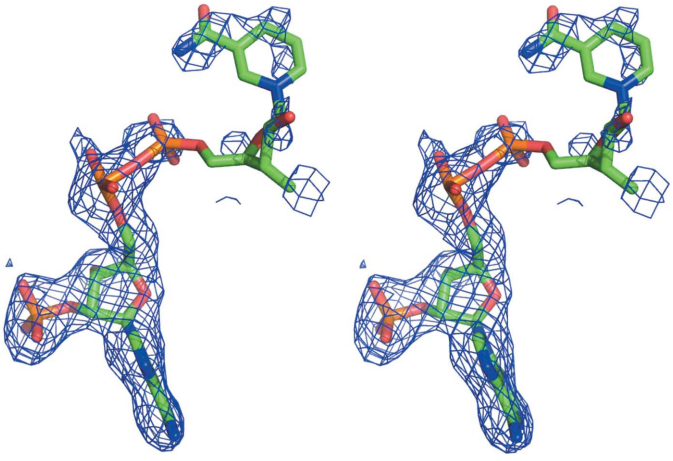

Figure 5
Stereo representation of NADPH. An $F_o - F_c$ OMIT map of NADPH is shown in stereo at a contour level of 1.0σ. The map was calculated by excluding NADPH from the model using *CNS*. Electron density for the nicotinamide-sugar portion is missing.

3.3. Comparison of the DXR structures

In order to clarify the difference between our structure and the ternary structure complexed with fosmidomycin and Mn^{2+} (PDB code 1onp), we superposed these two structures. When the two structures were fitted using the C^α-atom positions of the region spanning Thr4–Ala104, which is part of the NADPH-binding domain, the r.m.s.d. value of this region based on C^α-atom positions was 0.30 Å (Fig. 6). Interestingly, the central catalytic domains of both structures also matched very well, excluding the loop region (a green ellipsoid in Fig. 6) covering the active site, with an r.m.s.d. value of 0.26 Å. On the other hand, the loop region and the C-terminal domain showed differences, with r.m.s.d. values of 1.35 and 0.85 Å, respectively. Based on the position of the C-terminal domain, the NADPH domain and the C-terminal domain of the quaternary complex appear to be closer to each other than observed in the ternary complex structure; this feature may be an important component required for the correct positioning of ligands in the active site for catalysis.

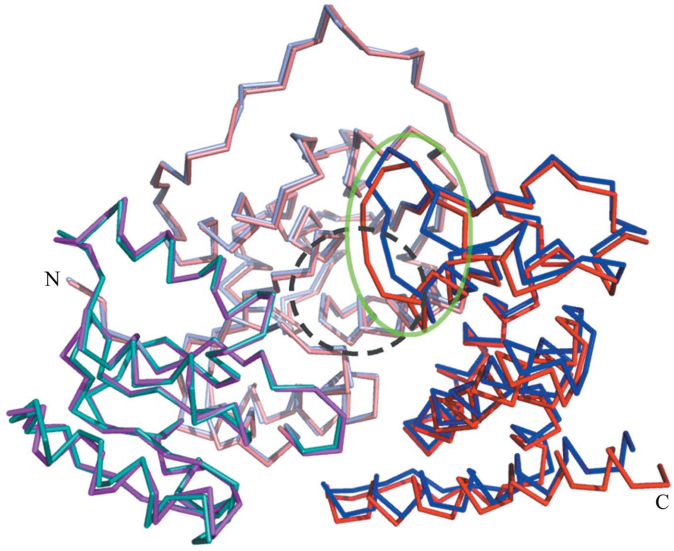

Figure 6
Superposition of two DXR structures. The superposed monomer structures are shown as C^α traces. The ternary complex of Mn^{2+} and fosmidomycin (PDB code 1onp) and the quaternary complex of Mg^{2+}, NADPH and fosmidomycin (this study) superposed based on the C^α-atom positions of Thr4–Ala104 are shown in cyan (ternary) and magenta (quaternary) on the left-hand side of the structures. On superposition, the central portions of the two structures (shown in pale blue and red for the ternary and quaternary structures, respectively) also matched well. In contrast, differences were observed between the right-hand portions (C-terminal domains) of the two structures, which are shown in blue and red for the ternary and quaternary structures, respectively. The broken circle indicates the position of the active site and the green ellipsoid shows the loop region covering the active site.

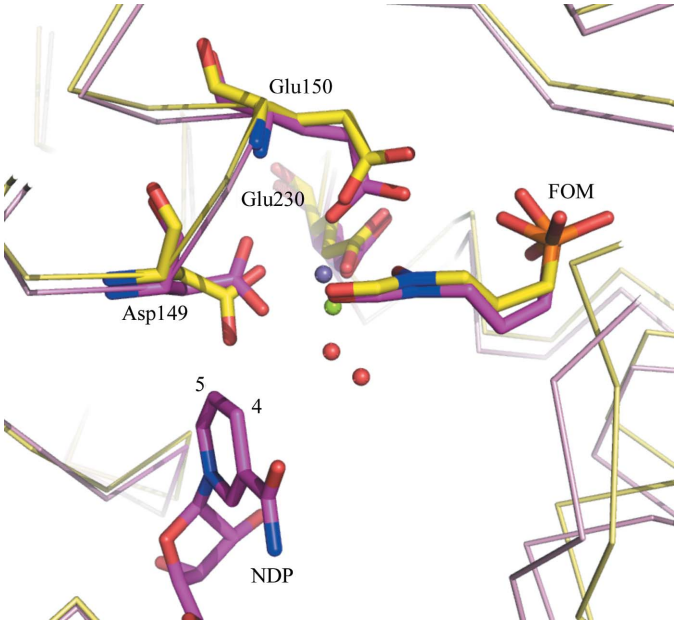

Figure 7
Residues in the active site after superposition of the ternary and quaternary complexes, which are coloured yellow and pink, respectively. The purple and green spheres represent Mn^{2+} (the ternary complex) and Mg^{2+} (the quaternary complex), respectively. Water molecules are shown as red spheres. NADPH in the quaternary complex is labelled NDP.

In the active site, the side chain of Asp149 of the quaternary complex appears to be displaced from its position in the ternary complex (Fig. 7). The resolution of the ternary structure is 2.6 Å and the *B* factors of Mg^{2+} and the ligands were higher than those of the protein residues in the quaternary structure; thus, the small differences in the position of Asp149 may not be significant. However, one possibility for this observation is that it is caused by the NADPH binding, as the side chain of Asp149 in the ternary complex is located very close to the potential position of the nicotinamide ring. This difference might affect the position of the metal ions. Mn^{2+} and Mg^{2+} are also located at different positions, although the O atoms in the (*N*-formyl-*N*-hydroxy)amino group of both structures matched well. Thus, the difference between the two structures resulted from a shift in the position of the side chain of Asp149 and/or the different binding properties of the two metal ions.

When we compared the relative positions of the NADPH domains and C-terminal domains of three DXR structures, *i.e.* the ternary complexes with Mn^{2+} and fosmidomycin (PDB code 1q0q) and with NADPH and fosmidomycin (1onp) and the quaternary complex investigated in this study, all three structures exhibited differences in the relative orientations of their domains and this is reflective of the structural flexibility of the DXR conformation.

We thank the staff of the Photon Factory for assistance during data collection.

References

Brünger, A. T., Adams, P. D., Clore, G. M., DeLano, W. L., Gros, P., Grosse-Kunstleve, R. W., Jiang, J.-S., Kuszewski, J., Nilges, M., Pannu, N. S., Read, R. J., Rice, L. M., Simonson, T. & Warren, G. L. (1998). *Acta Cryst.* D**54**, 905–921.
DeLano, W. L. (2002). *The PyMol Molecular Visualization System.* http://www.pymol.org.
Henriksson, L. M., Bjorkelid, C., Mowbray, S. L. & Unge, T. (2006). *Acta Cryst.* D**62**, 807–813.
Jomaa, H., Wiesner, J., Sanderbrand, S., Altincicek, B., Weidemeyer, C., Hintz, M., Türbachova, I., Eberl, M., Zeidler, J., Lichtenthaler, H. K., Soldati, D. & Beck, E. (1999). *Science*, **285**, 1573–1576.
Kuzuyama, T. & Seto, H. (2003). *Nat. Prod. Rep.* **20**, 171–183.
Kuzuyama, T., Shimizu, T., Takahashi, S. & Seto, H. (1998). *Tetrahedron Lett.* **39**, 4509–4512.
Kuzuyama, T., Takahashi, S., Takagi, M. & Seto, H. (2000). *J. Biol. Chem.* **275**, 19928–19932.
Kuzuyama, T., Takahashi, S., Watanabe, H. & Seto, H. (1998). *Tetrahedron Lett.* **39**, 7913–7916.
Laskowski, R., MacArthur, M., Moss, D. & Thornton, J. (1993). *J. Appl. Cryst.* **26**, 283–291.
Lell, B., Ruangweerayut, R., Wiesner, J., Missinou, M. A., Schindler, A., Baranek, T., Hintz, M., Hutchinson, D., Jomaa, H. & Kremsner, P. G. (2003). *Antimicrob. Agents Chemother.* **47**, 735–738.
Mac Sweeney, A., Lange, R., Fernandes, R. P., Schulz, H., Dale, G. E., Douangamath, A., Proteau, P. J. & Oefner, C. (2005). *J. Mol. Biol.* **345**, 115–127.
Otwinowski, Z. & Minor, W. (1997). *Methods Enzymol.* **276**, 307–326.
Reuter, K., Sanderbrand, S., Jomaa, H., Wiesner, J., Steinbrecher, I., Beck, E., Hintz, M., Klebe, G. & Stubbs, M. T. (2002). *J. Biol. Chem.* **277**, 5378–5384.
Ricagno, S., Grolle, S., Bringer-Meyer, S., Sahm, H., Lindqvist, Y. & Schneider, G. (2004). *Biochim. Biophys. Acta*, **1698**, 37–44.
Rohmer, M. (1999). *Nat. Prod. Rep.* **16**, 565–574.
Sacchettini, J. C. & Poulter, C. D. (1997). *Science*, **277**, 1788–1789.
Steinbacher, S., Kaiser, J., Eisenreich, W., Huber, R., Bacher, A. & Rohdich, F. (2003). *J. Biol. Chem.* **278**, 18401–18407.
Takahashi, S., Kuzuyama, T., Watanabe, H. & Seto, H. (1998). *Proc. Natl Acad. Sci. USA*, **95**, 9879–9884.
Wiesner, J., Borrmann, S. & Jomaa, H. (2003). *Parasitol. Res.* **90**, *Suppl.* 2, S71–S76.
Yajima, S., Hara, K., Sanders, J. M., Yin, F., Wiesner, J., Jomaa, H., Ohsawa, K. & Oldfield, E. (2004). *J. Am. Chem. Soc.* **126**, 10824–10825.
Yajima, S., Nonaka, T., Kuzuyama, T., Seto, H. & Ohsawa, K. (2002). *J. Biochem. (Tokyo)*, **131**, 313–317.